https://doi.org/10.1016/j.cej.2022.137772

pH-sensitive Thermally Regenerative Cell (pH-TRC) with Circulating Hydrogen for Long Discharging Time and High-Power Output

Chun Cheng [a&], Sijia Wang [b&], Yifan Wu [c], Tong Liu [a], Shien-Ping Feng [b,d,*] & Meng Ni [a,*]

[a] Department of Building and Real Estate, Research Institute for Sustainable Urban Development (RISUD) & Research Institute for Smart Energy (RISE), The Hong Kong Polytechnic University, Hung Hom, Kowloon, Hong Kong, China

[b] Department of Mechanical Engineering, The University of Hong Kong, Pokfulam Road, Hong Kong, China

[c] Institute of New Energy and Low-Carbon Technology, Sichuan University, Chengdu, China

[d] Department of Advanced Design and Systems Engineering (ADSE), City University of Hong Kong, Tat Chee Avenue, Kowloon, Hong Kong, China

* Shien-Ping Feng: tony.feng@cityu.edu.hk

* Meng Ni: meng.ni@polyu.edu.hk

Highlights

- A robust and scalable approach for low-grade waste heat to electricity.
- Voltage by anolyte/catholyte pH difference was regenerated by thermal distillation.
- About 5 Wm^{-2} of power density and 21,000 seconds of discharging time were obtained.
- Model was validated and performed for a better cell engineering.

Abstract

Thermally Regenerative Cell (TRC) is a recently proposed promising approach for converting low-grade waste heat into electricity, but the power density and discharging time are limited by the loss of electrode active material and unoptimized cell design. By replacing the early consumable electrode with H_2/H^+ catalytic electrode and rationally improving the cell design, here we report an advanced pH-sensitive thermally regenerative cell (pH-TRC) with circulating hydrogen to achieve both long discharging time and high-power output. Between the H_2/H^+ catalytic electrodes we have flowing anolyte and catholyte with different various pH values, which can be neutralized through discharging reactions and then thermally regenerated to reset the initial state. With this new design, a favorable peak power density of 5.296 W m^{-2} is obtained. More importantly, an incredibly long discharging time over 40 hours enables the powering of a smart phone in comparison to only hundreds-of-seconds discharging time of previous TRC.

Graphical abstract

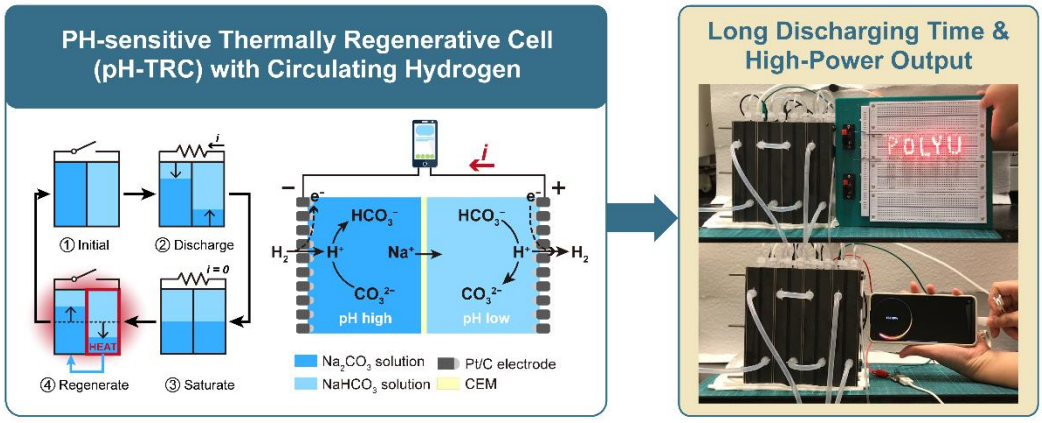

Keywords

low-grade heat harvesting; pH-sensitive thermally regenerative cell; circulating hydrogen

1. Introduction

Low-grade heat (<100℃) harvesting has become an urgent challenge under environmental crisis since a large proportion of waste heat cannot be effectively utilized by traditional heat engines [1–3]. Owing to the significant potential to harvest energy from low-grade heat, liquid-based electrochemical systems have attracted tremendous research interests in heat-to-electricity energy conversion [4,5]. The most widespread approach among liquid-based electrochemical systems, thermal galvanic cell (TGC), can directly generate electricity from spatial temperature gradient. However, the spatial temperature gradient diminishes quickly due to heat convection and conduction, leading to an unsustainable open circuit voltage (OCV) and a short discharging time of only a few hundred seconds [6–11]. To address this issue, electrolytes with low heat conductivity and high electric conductivity are favored. Nevertheless, these two parameters can hardly be decoupled, resulting in short discharging or an unsatisfactory power density, thereby greatly limiting the practical application of these non-isothermal cells.

To enable a long-run efficient heat-to-electricity conversion system, isothermal electrochemical cells utilizing chronological temperature gradient rather than spatial temperature gradient are emerging, which can be characterized as thermally regenerative cells (TRCs) [5]. These cells relying on a Gibbs free energy storage from thermal cycle rather than thermal gradient directly deliver electricity as external work. To be more precise, these systems, including thermally regenerative electrochemical cycles (TRECs) [12–15], direct thermal charging cells (DTCCs) [16,17], thermally regenerative ammonia batteries (TRABs) [18–20], and thermally regenerative CO_2-induced pH-gradient cell (TRCPC) [21], operate within a certain temperature range, discharging at T_1 and regenerating at T_2. TRECs and DTCCs rely on different cathode and anode with different temperature coefficients, generating electricity from temperature cycles. On the contrary, TRABs and TRCPCs apply same cathode and anode but different catholyte and anolyte that can be regenerated by low-grade waste heat. Our previous work on TRCPC demonstrated a new concept by using thermally regenerative pH-gradient and pH-sensitive electrodes for heat-to-electricity conversion, here classified as pH-sensitive thermally regenerative cells (pH-TRCs). Fig. 1a shows the mechanism of a pH-TRCs to convert heat to electricity. OCV (black line) represents Gibbs free energy difference (ΔG, blue line) between the initial state (before discharging) and final state (after discharging) and can be expressed as $OCV=-\Delta G/nF$ [15], where n is the electrons transferred from electrochemical reaction, F is the Faraday constant. Capable of discharging, the output electric work can be evaluated to be ideally equal to ΔG. During discharging, the OCV gradually reduces to zero, with a simultaneous decrease in ΔG. Once ΔG is fully exploited during discharging, it will then be regenerated into initial state in a following thermal regeneration step,

corresponding to increases in energy and OCV. Theoretically, pH-TRCs' working mode potentially can achieve both endurable discharging and satisfactory power density.

Previous TRCs focus on the electrode-involved electrochemical reactions (such as intercalation and deintercalation of alkali metal ions, metal complexation reaction) [12–15,18–21]. The consumption of active materials heavily restricts the lifetime of the electrodes. Therefore, most of the research remains in the stage of experimental verification, far too little attention has been paid to longer the discharging time with a good power for demonstrable use. In approaching this aforementioned issue, platinum-H_2/H^+ catalytic electrodes were designed to replace the consumable electrodes, and then applied in a proposed pH-TRC with circulating hydrogen. Figure 1b and 1c show the working mechanism of the design. First, the pH-TRC consists of anolyte (0.5 M Na_2CO_3, pH=11.70) and catholyte (1 M $NaHCO_3$, pH=8.30) with different pH values, allowing an initial pH-induced potential built between the symmetric platinum-H_2/H^+ catalytic anode and cathode. To be noticed, $Na_2CO_3/NaHCO_3$ electrolytes were selected because of their great adaptability in combination with carbon capture and storage (CCS) technologies, giving potential to a cost-effective and scalable system that utilizes wastes (CO_2 and low-grade heat) to produce electricity without external energy supply [21,22]. Next, when the anode and cathode experience reversed proton-related reactions on platinum-H_2/H^+ catalytic electrodes respectively, anolyte and catholyte are neutralized accordingly and this discharging process is ended with an equal pH value of anolyte and catholyte. It should be noted that Na^+ dominates the ion transport in electrolytes due to the relatively low concentration of H^+. Also, despite of no Na^+ concentration gradient between anolyte and catholyte, Na^+ is still able to cross through a CEM by migration under an electric field rather than diffusion. Then, the electrolytes are

regenerated by heat to subsequently establish a renewed potential. As a result, a full cycle of pH-TRC is achieved by resetting the pH values of electrolytes as depicted in Fig. 1b. This cycle briefly comprises discharging process and regeneration process, individually terminated at saturated and initial state.

The cell structure of pH-TRC with circulating hydrogen is demonstrated in Fig. 1c. Symmetric platinum-H_2/H^+ catalytic electrodes are initially immersed into anolyte of 0.5 M Na_2CO_3 and catholyte of 1 M $NaHCO_3$ separately (Fig. 1a). The hydrogen gas flows via gas channel meanwhile electrolytes flow through flow channel, where the two channels are sealed by silicone sheets and separated by catalytic electrodes. Reactions occur at the surface of platinum-H_2/H^+ catalytic electrode thereby producing electrons, which are conducted to graphite electrode holder, and ultimately to copper current collector for external circuit power supply.

In this study, power density, discharging time and efficiency of pH-TRC were carefully investigated by both experimental results and theoretical computations. It is shown here that the pH-TRC demonstrates an incredibly long discharging time with a satisfactory power density.

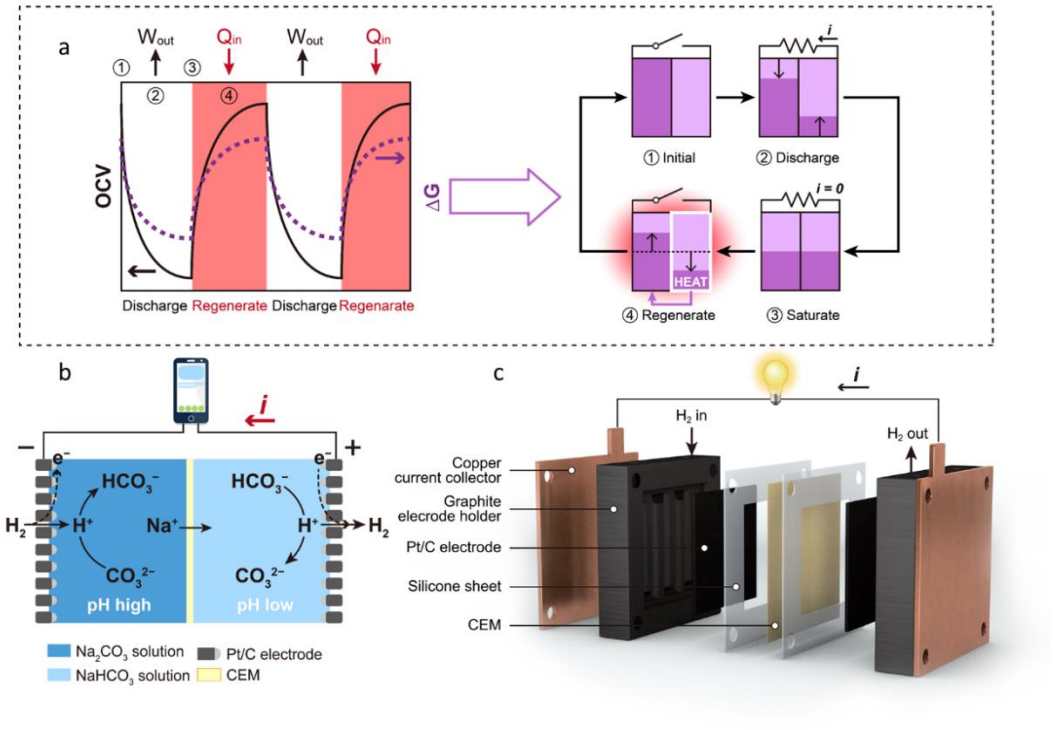

Figure. 1 Working mechanism of pH-TRC to convert heat into electricity. (a) Schematic of typical TRC; (b) Schematic of pH-TRC; (c) Single cell structure of pH-TRC.

2. Experiment section

2.1. Materials

Pt/C powder (20%, XC-72r Pt/Vulacan, Premetek), Sodium carbonate (Na_2CO_3, ACS, 99.5%, Aladdin), sodium bicarbonate ($NaHCO_3$, HPLC, ≥ 99.8%, Aladdin), Nafion solution (5%, D520, Dupont), polytetrafluoroethylene solution (60%, D210C, Daikin), carbon paper (28BC, Sigracet), carbon cloth (1011, CeTech), were used without further treatment or purification.

2.2. Preparation of Pt/C electrodes

For the carbon paper electrodes, 20 mg Pt/C powder (20%), 0.053 g Nafion solution (5%) and 0.0044 g PTFE solution (60%), was mixed and dissolved in 1 mL water-

isopropanol mixture (1:4). The Pt/C ink was obtained after 30 min sonication and sprayed on a piece of 2 cm × 2 cm carbon paper at 120 ℃ for several times. For the carbon cloth electrodes, 20 mg Pt/C powder (20%), 0.0707 g Nafion solution (5%) was mixed and dissolved in 1 mL water-IPA mixture (1:4). After 30 min sonication and ink spraying, the obtained electrodes were heated at 120 ℃ in an oven for 2 hours. Scanning electron microscope (SEM) images of anode and cathode are shown in supporting information Fig. S1.

2.3. pH-TRC system configuration and operation

The construction of single pH-TRC was carried out by assembling the Pt/C electrodes (2×2 cm), CEM (4×4 cm), two flow channels (4×4×0.1 cm, fluor rubber sheets), two electrode holders (4×4×1.5 cm, graphite) with two gas channels (2×2×0.15 cm), two current collectors (4×4×0.1 cm, copper), and two end plates (4×4×1 cm, titanium). The Pt/C electrodes were prepared by spraying Pt/C ink to carbon paper (anode) and carbon cloths (cathode) with an even loading mass of 1 mg Pt per cm^2. The electrodes were tightly glued by liquid rubber to the electrode holders to form the whole electrodes. After drying, the electrodes were connected to the current collectors by adhesive-back fluor rubber sheets and thereby connected to the titanium end plates, fixed by bolts and nuts. The electrolytes were prepared to be 1 M $NaHCO_3$ and 0.5 M Na_2CO_3 by using ultrapure water and then pumped into the cell as catholyte and anolyte. The electrodes, flow channels and membranes increased but remained the other fixing components for series and parallel configurations of multiple cells. Since each adjacent cell was separated by insulating gasket, cells could be arranged in rows, meeting various discharging modes by changing connections. It is worth

mentioning that although the main substances (Na_2CO_3 and $NaHCO_3$) initiating the pH-gradient are very cheap (*ca.* 0.014 USD g^{-1} and 0.018 USD g^{-1}, respectively) the major cost of a single pH-TRC device in the experiment comes from the Pt/C electrodes (*ca.* 0.771 USD cm^{-2}) and the graphite/copper/titanium current collector with gas channels (*ca.* 0.215 USD cm^{-2}).

2.4. Characterization

The electrochemical tests were performed on CHI 760E electrochemical workstation (CH Instrument, Shanghai). The SEM images were captured by VEGA3 (Tescan). The gas chromatography curves were recorded on GC9720 (Fuli Instruments).

3. Results and discussion

3.1. Open circuit voltage (OCV) generation

It is crucial to understand the generation of OCV since it implies reactions occurring on electrodes. With a hydrogen supply to the anode, electricity is derived from reversible pH-driven electrode reactions as expressed below.

Anode: 0.5 M Na_2CO_3

$$H_2 \rightarrow 2H^+ + 2e^- \quad (1)$$

$$2H^+ + 2{CO_3}^{2-} \rightarrow 2{HCO_3}^- \quad (2)$$

Cathode: 1 M $NaHCO_3$

$$2H_2O + 2e^- \rightarrow 2OH^- + H_2 \quad (3)$$

$$2OH^- + 2{HCO_3}^- \rightarrow 2{CO_3}^{2-} + 2H_2O \quad (4)$$

During discharging, the anode and cathode experience the hydrogen oxidation reaction (HOR) and the hydrogen evolution reaction (HER), respectively, the net H_2 consumption is zero. Theoretically, OCV established by a pH difference between the anolyte and the catholyte would gradually decrease from approximately 0.2 V to 0 V when an equal-pH-state is reached (Fig. 2a, b). Afterward, thermal regeneration of electrolytes can be conducted to initialize the discharging state. It is worth noticing that the number of theoretical electrons transferred through the aforementioned reaction is not 1 M or 0.5 M but much lower. Considering the product and anion migration effect on the pH difference, the transferred electrons are determined to be 0.32 M. Therefore, 1.426 KJ of electricity can be generated corresponding to 1 L anolyte/catholyte.

Corresponding to the aforementioned reactions of the anode and cathode, a theoretical OCV can be determined as below, assuming the standard states for gas and solutions are 1 atm and 1 M. From the OCV equation, it suggests that OCV value is contributed by differences in both pH and hydrogen partial pressure, which is clearly illustrated in Fig. 2c. The OCV of the cell stabilized at 0.17 V at the beginning and increased significantly until it rapidly reached a peak voltage of over 1 V within a few seconds once the cell was supplied with hydrogen. This value gradually decreased to 0.2061 V in the end.

$$OCV = 0.059\left(pH_a - pH_c + lg\ p_{H_2c}^{0.5} - lg\ p_{H_2a}^{0.5}\right) \quad (5)$$

The outset and end of voltages suggests that the OCV value is mainly determined by the pH difference since there is only a slight increase of 0.306 V (Fig. 2c) in

the OCV after gas supply on comparison to the OCV of 0.13 V caused by the pH difference at the start (Fig. 2c). However, it still couldn't explain the peak and slope of OCV. To explore the causes of the peak and slope of OCV, the electrode potentials of anode and cathode were respectively measured in 0.5 M Na_2CO_3 and 1 M $NaHCO_3$ in a proper order. Fig. 2d and 2e depict the OCV changes of anode and cathode corresponding to switching inlet H_2. The values of the anode and cathode OCV both start at a positive value, but end at a negative value after providing H_2, suggesting an additional oxygen reduction reaction (ORR) from the dissolved oxygen, which dominates the OCV at the start. However, with saturation of H_2 in electrolyte, the voltage changes into normal values at -0.7256 V of anode and -0.5206 V of cathode, providing an overall OCV of 0.2 V at the end, which confirms the final OCV in Fig. 2c. Besides, the anode (carbon paper) displays a quicker response in comparison to cathode (carbon cloths) from Fig. 2d and 2e. That helps to illustrate an asymmetric peak OCV in Fig. 2c, where an extremely sharp OCV slope appears before the peak value and slowly fades afterward. The effect of dissolved H_2 on OCV was further investigated by examining the cathode in different electrolyte states. The cathode was immersed in 1 M $NaHCO_3$, 0.5 M Na_2CO_3 and 1 M $NaHCO_3$ in turn, which contained dissolved H_2. Then the electrolyte underwent an intense shake to expel the hydrogen adsorbed on the electrode surface, followed by a H_2 supply again. As seen from Fig. 2f, a 0.2 V voltage change from -0.52 V to -0.72 V appears after altering electrolyte, which confirms our speculation. Later, the voltage was initiated by replacing the electrolyte into the original electrolyte of 1 M $NaHCO_3$ with saturated H_2. After which, the voltage increases at an alarming rate and returns to the initial voltage because of the vibration in H_2 concentration. Owing

to the low partial pressure of H_2 (< 1 atm) in an exponential form, a minor change in H_2 concentration leads to dramatic changes in OCV, which is consistent with the aforementioned OCV equation. The foregoing results further confirm the need to ensure sufficient hydrogen concentration in the catholyte solution at the beginning. Otherwise, a false OCV would be produced. For this reason, H_2-saturated electrolytes were applied in all experiments if not otherwise stated.

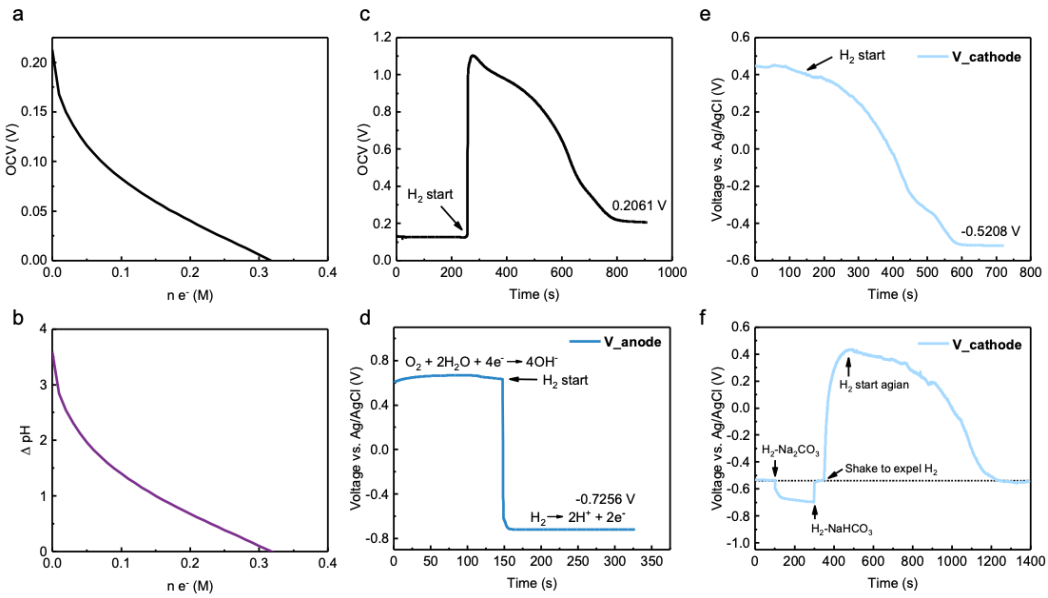

Figure. 2 Open circuit voltage (OCV) change in pH-TRC. (a) The OCV and (b) pH difference change with electron transfer during discharging; (c) OCV of cell, (d) anode and (e) cathode change by hydrogen supply; (f) Voltage change with electrolyte state.

3.2. Working characteristics of pH-TRC

After investigating the OCV generation, the discharging ability of pH-TRC was evaluated in this section. To properly understand the working characteristics, the linear sweep voltammetry (LSV) experiments were conducted in a single cell to study the discharging abilities of anode and cathode. LSV results of cathode and

anode are shown in Fig. 3a and 3b separately, where dashed line represents initial OCV. In Fig. 3a, it is noticeable that two plateaus perform H_2 and OH^- diffusion dominated process as the voltage shifts negatively. Due to the low OCV, the cathode potential cannot be shifted to -0.8 V, thus the discharging process in cathode is unlikely to be controlled by OH^- diffusion. Regarding to the anode, the discharging process is much more complicated, as it involves complicated H-adsorption, which is a cause for fluctuations existing in LSV curve of the cathode.[23] Curves relating overpotential to *lg j* (anode and cathode) are given in Fig. 3c. The power density limit can be drawn by comparing current densities of anode and cathode under a same absolute value of overpotential, respectively. Given an overall OCV of 0.2 V, the current density of cathode is 5 times higher than that of anode within an overpotential range of 0 to 0.2 V. That means it is easier to reach cathode maximum current density than anode maximum current density. Briefly, it can be concluded that the power density is limited by anode. That is not only owing to the relatively complicated H-adsorption in anode, but also related to the substrate material of the electrode, since cathode of hydrophilic carbon cloth provide larger reaction area than that of anode with a hydrophobic carbon paper substrate. A pH-TRC generates a peak power density of 5.296 W m^{-2} in Fig. 3d, which satisfies the practical power requirements of devices in general. As a proof-of-concept, four cells (each electrode surface of 10×10 cm) connected in parallel are capable of powering a smart phone and a LED array as demonstrated in Fig. 3e and 3f respectively. The demonstrations were conducted under a gas flow rate of 5 mL min^{-1} and an electrolyte flow rate of 40 mL min^{-1}. Two shared reservoirs to store anolyte and catholyte, respectively, allow the circulation and further regeneration of flowing electrolyte. A booster circuit was applied to adjust

the output voltage without changing the absolute power output.

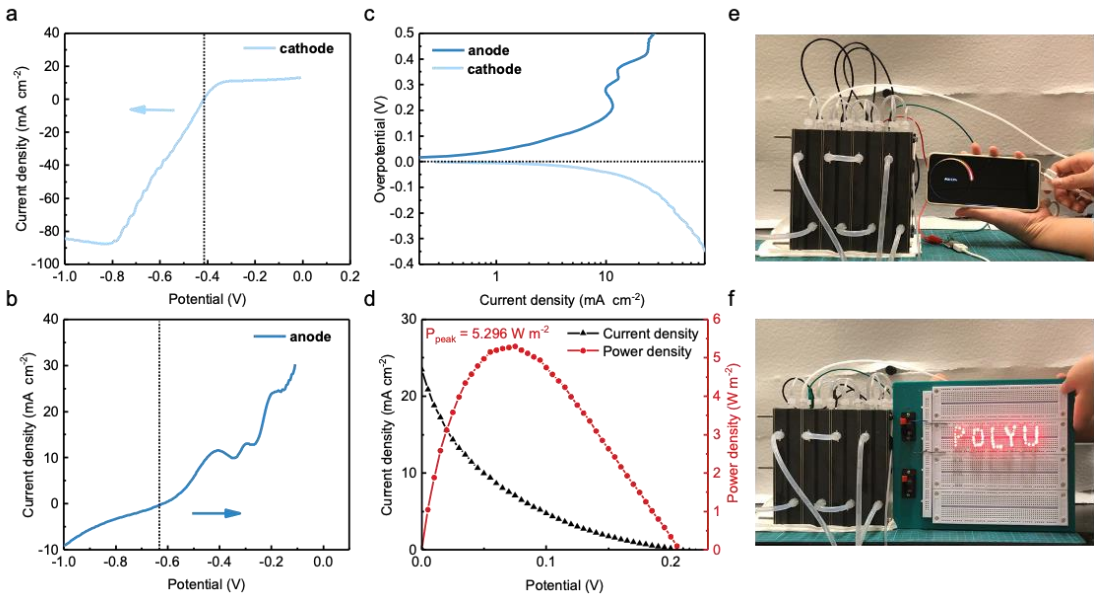

Figure. 3 Results in power. (a-c) LSV results of anode and cathode at sweep speed of 5 mV s^{-1}; (d) Power density of a single cell pH-TRC (electrolyte flow rate: 40 mL min-1, gas flow rate: 5 mL min-1); (e-f) Demonstrations of pH-TRC powering a smart phone and LED array.

3.3. System stability and effect of operation temperature

The total energy of pH-TRC is directly related to the electrolyte volume. Firstly, electricity production by a single cell was examined with 1.2 mL of still anolyte and 2 L of flowing catholyte ($V_{anolyte} << V_{catholyte}$). Fig. 4a shows the discharging process in stages under the current from 10 mA to 1 mA, which provided a long-standing discharging time of over 21000 of seconds with a capacity of 15.53 mA h. In this case, the amount of catholyte is infinite enough to accommodate the transferred sodium ions, the resultant anolyte and catholyte will both be pure $NaHCO_3$. Fig. 4b gives a proof of equal pH values (~8.5) of anolyte (left hand) and catholyte (right hand) by precise pH strips (5.5 - 9.0) after discharging. That

implies 0.5 M electrons transferred in the case of Fig. 4a. Accordingly, a theoretical capacity of 16 mA h can be determined in this case, closely approaching our experimental result (15.53 mA h). On the other hand, if the same volume of anolyte and catholyte ($V_{anolyte} \approx V_{catholyte}$) are provided, the resultant products will be a mixture of Na_2CO_3 and $NaHCO_3$. Fig. 4c plots the pH change trends of anolyte and catholyte with a same volume in discharging process. If the cation effect on pH is carefully taken into account, the transferred electrons are estimated to be 0.3 M. To further illustrate this point, a discharging experiment with the same 50 mL of electrolytes was conducted (Fig. 4d). Consequently, electricity of 0.2046 A h was generated within an extremely appealing long discharging period of over 170 thousand of seconds. The corresponding energy density of anolyte was 4.092 Ah m^{-3} ($V_{anolyte} \approx V_{catholyte}$) lower than 13.333 Ah m^{-3} ($V_{anolyte} << V_{catholyte}$) in the first case (Fig. 4e) as a result of incomplete conversion from Na_2CO_3 to $NaHCO_3$, which follows the prediction.

As our previous work suggested that increasing operating temperature during discharging might be beneficial, power densities at different temperatures were evaluated, where the peak power densities and a discharging curve at 50℃ were given in Fig. 4e and g, respectively. The power densities at higher temperatures are evidentially higher than those at lower temperatures. However, the energy density decreased under higher temperature. A single cell at 50℃ provides only 60% capacity of that at 25 ℃, suggesting the opposite effects of temperature on power density and capacity. A potential reason could be the electrolyte decomposition at higher temperature during discharging, while the consequently volatilized CO_2 reduces pH differences and thereby causing capacity loss. To

confirm this speculation, the produced gas catholyte was collected and compared with standard H_2 and CO_2. The gas chromatography results (Fig. 4h) evidently showed that the produced gas was a mixture of H_2 and CO_2. Therefore, a higher operation temperature is not favored in the long run.

However, that doesn't mean no electrolyte decomposition occurs at room temperature. Even though considering the aforementioned differences in transferred electrons in cases of Fig. 4a and 4d, the energy density shown in Fig. 4a is still twice of that in Fig. 4b. This result can be attributed to the difference in discharging time, where little decomposition occurred in a shorter discharging time.

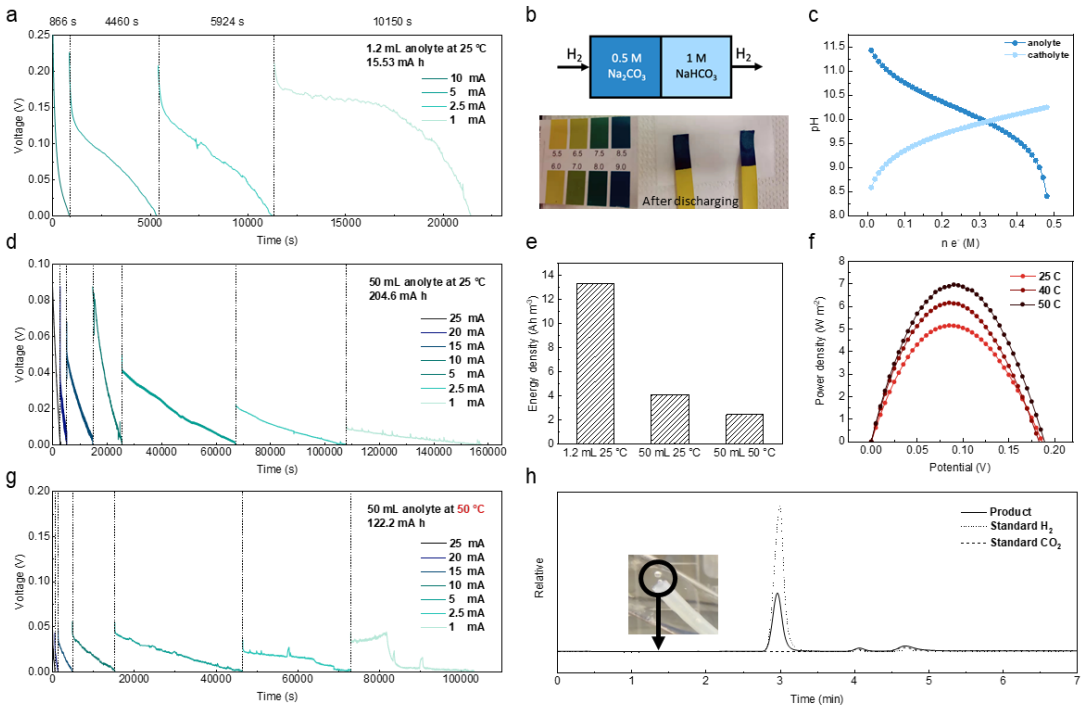

Figure. 4 Discharging performance at room temperature and higher temperature. (a) Discharging curve with 1.2 mL anolyte and 2 L catholyte at room temperature; (b) Mechanism of pH value change of electrolytes during discharging, and

comparison of anolyte and catholyte after long-time discharging; (c) Calculated pH value change of electrolytes during discharging; (d) Discharging curve with 50 mL anolyte and 50 mL catholyte at room temperature; (e) Comparison of energy density with different electrolyte volume and temperature; (f) Power densities with different temperatures; (g) A discharging curve with equal volume of 50 mL of electrolytes at 50 Celsius; (h) Gas chromatography curve of discharging product from catholyte.

3.4. Effect of flow rate and supporting electrolyte

To evaluate the effect of flow rate on power density, a comprehensive mathematical model was developed to simulate the transport and electrochemical process in a pH-TRC. The model was validated by comparing the experimental and computational peak power density in Fig. 5a. It shows a good agreement between the simulation (4.953 W m^{-2}) and experimental data (5.296 W m^{-2}). A minor shifting is due to the acceptable errors from calculation in experimental exchange current density. After model validation, parametric simulations were conducted to understand the effects of various operational parameters on pH-TRC performance. Fig. 5b and 5c provide experimental and computational power densities under various gas flow rates and electrolyte flow rates (assuming equal flow rates of anolyte and catholyte) respectively. Both experimental and computational power densities stabilize at approximately 5 W m^{-2} in Fig. 5b, as those sufficient reactants are supplied in this condition regardless of flow rate.

However, the same is not true for different electrolyte flow rates. The computational power density increases significantly from 2.53 to 4.07 W m^{-2}

within the flow rate of 0.1 to 10 mL min^{-1}, subsequently rises slowly to 5 W m^{-2}. The experimental results well fit the computational results, proving the pH-TRC experience two different dominant steps with an accelerating flow rate. They are mass transfer step at low flow rate and reaction kinetic step under sufficient mass transfer. When the reaction transitions from mass transfer to reaction rate controlled, there is a correspondingly noticeable change in current density. That well explained the curve trends in Fig. 5c.

As is obvious from previous discussion, electrolyte flow rate is an important factor affecting power density. Yet it would be negligent not to consider the auxiliary input power from pump. The pump powers are given in Fig. 5d with a pump efficiency of 5%, suggesting applicable flow rates in terms of different power density generated from a pH-TRC. The mean power densities were calculated from a typical discharging case in Fig. 4d. As a gradual decrease in power density in a continuous discharging process, a cascade strategy was developed to reduce additional input energy. That is, applying high flow rate at the beginning and switching to low flow rate gradually, which helps achieve a high relative efficiency of 22.595% in this case (related to an idea efficiency of 0.27%). The energy efficiency of different low-grade heat harvesting systems including TRECs, DTCC, TRABs, and pH-TRC are compared in Supplementary Note 1, and the detail of the calculation is showed in Supplementary Note 2.

Interestingly, the peak power density seldomly changes by adjusting other parameters including diffusion coefficient in gas diffusion layer etc., except for changing the exchange current density of anode (noting here $j_0 = nFk^{\circ}$, where

j_0 is the exchange current density, k° is the standard rate constant, a larger exchange current density corresponds to a higher electrode activity). Fig. 5e shows a stable increase in power density with increasing exchange current density of anode. As noted previously, the power density is mainly limited by the anode. Therefore, optimizing the anode reaction kinetics could be more effective than structure design. This problem may potentially be improved in three ways: First, optimize the electrode catalytic materials. Since the catalytic sites of platinum are mainly on the Pt (111) surface, it may be possible to use the electrochemical method to deposit platinum on the electrode with more catalytic sites. Second, adjust the products. The cathodic reaction rate can be possibly increased by introducing precipitation reaction relative to CO_3^{2-} (enlarging the local reactant/product concentration difference). Third, optimize the reaction conditions. We have found the anode reaction favours a higher flow rate of the anolyte. This is because the fresh anolyte can neutralize the newly generated hydrogen ions. Therefore, a flowing regenerative electrolyte with a higher pH may be helpful.

In addition to the aforementioned parameters, power production with different concentrations of supporting electrolyte is also estimated in Fig. 5f. It is supposed that sodium sulfate was added into electrolyte to reduce the internal resistance without changing the pH values of electrolytes. However, an unexpected decrease in power density is found with supporting electrolyte in Fig. 5f. In view of these observations, it is quite likely that anion adsorption at platinum electrode surfaces obstructs HOR/HER reactions, which has been proved in references[24–27]. It is worth mentioning that, considering a higher concentration of sodium bicarbonate solution produces a larger pH difference between the anolyte and catholyte,

and less amount of water needs to be heated given the same amount of reactants thereby reducing the heat loss, higher concentrations are favoured in this system design. Therefore, there is an optimal concentration choice limited by the solubility of both Na_2CO_3 and $NaHCO_3$. The constant concentrations of Na_2CO_3 and $NaHCO_3$ in this work is attributed to this.

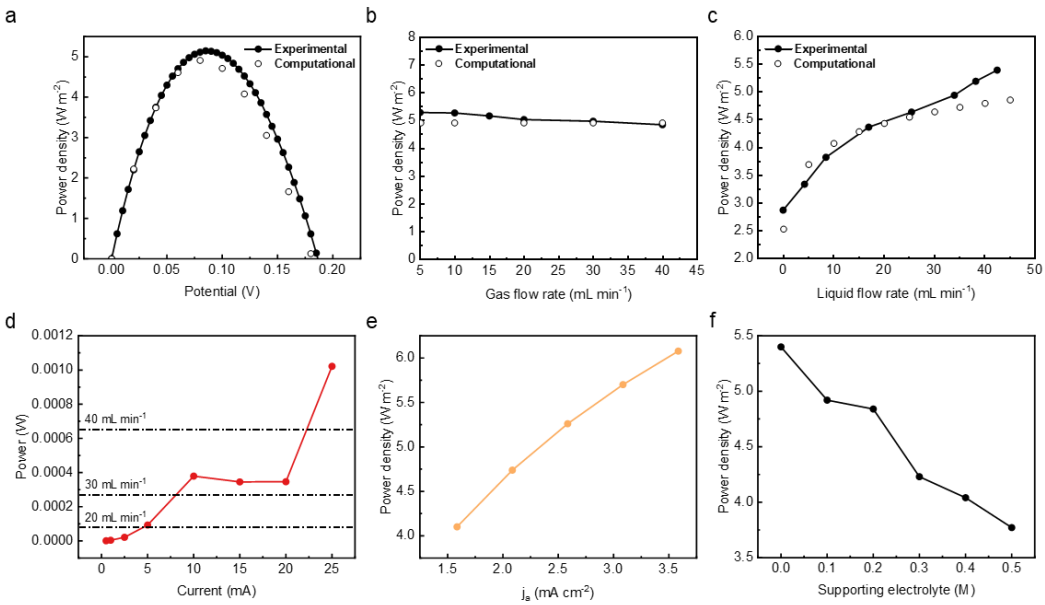

Figure. 5 Effects of flow rate, supporting electrolyte and exchange current density of anode. Comparison of experimental and computational power densities with (a) various working voltage, (b) different gas flow rate, and (c) different electrolyte flow rate; (d) Powers generated by a pH-TRC of 2×2 cm electrode area under different discharging current, where pumping powers under various electrolyte flow rate are plotted in dash line, suggesting a reasonable flow rate under a certain discharging current; (e) Power density changes with exchange current densities of anode and (f) a range of concentrations of supporting electrolyte. The model details are given in Supplementary Note 3.

3.5. Challenges and future perspectives of pH-TRC

Despite the high-power density and long discharging time achieved, pH-TRCs are still at its early development stage with relatively low energy conversion efficiency. There are three key components/issues in a pH-TRC: pH sensitive electrodes, thermally regenerative electrolytes, and a membrane to separate catholyte and anolyte. In this work, platinum-H_2/H^+ catalytic electrodes and $Na_2CO_3/NaHCO_3$ electrolytes were selected to replace previous consumable electrodes and to potentially integrate with CCS technologies, respectively. However, results show that the power was still limited by the relatively low anode reaction kinetics. Nevertheless, in addition to some of the improvements mentioned earlier, there are plenty of choices of other existing redox or pseudocapacitive materials that can be used as pH-sensitive electrodes in pH-TRCs, such as manganese (IV) oxide/manganese (III) oxyhydroxide (MnO_2/MnOOH), nickel (II) hydroxide/nickel oxide hydroxide ($Ni(OH)_2$/NiOOH), nickel hexacyanoferrate (NiHCF), and polyaniline (PANI), etc. As to thermally regenerative electrolytes, potential candidates including potassium carbonate (K_2CO_3), trisodium phosphate (Na_3PO_4), and sodium acetate (CH_3COONa), *etc*., may improve reaction kinetics by creating various pH environments Then, a proper membrane can be selected based on the electrode and electrolyte to facilitate desired ion transport. Apart from the variety of materials, cell/system structure also plays a vital role in approaching applications since the mass and heat transfer in a thermal regeneration process are mainly affected by the structure design. To sum up, as a new type of waste heat recovery platform, the current pH-TRC has plenty of room for optimization in the future from material to structural design.

4. Conclusions

A pH-sensitive thermally regenerative cell (pH-TRC) with circulating hydrogen was

proposed and evaluated experimentally and theoretically in this work. The newly developed pH-TRC successfully converted low-grade heat into electricity with a peak power density of 5.296 W m^{-2}. More importantly, the discharging feasibility and cell scalability were experimentally confirmed with our optimization strategy of altering the electrode, changing the membrane, and applying flowing electrolytes. A proof-of-concept implement displayed an incredibly long discharging time of hundreds of thousands of seconds, thousands of times higher than the reported discharging time in the literature [21]. Additionally, the OCV generation was analyzed based on electrode reactions. The system stability and effects of operation temperature, flow rate, and supporting electrolytes were evaluated and discussed. From these results one can conclude that the electrolyte flow rate and reaction rate of the anode determine the discharging performance of pH-TRC, and supporting electrolytes might not be favored in electrolytes. Compared with structural improvement, electrodes with a higher rate constant are absolutely required. The significantly improved power output and discharging time paved the way for practical application of waste-heat to electricity conversion.

Acknowledgements

M. Ni thanks the support by Collaborative Research Fund (CRF) (Project No. C5031-20G) of Research Grant Council, University Grants Committee, HK SAR.

Contributions

C.C. conceived the project. C.C. and S.W. performed the testing, analysis, and interpretation of data. Y.W., T.L. contributed on resources and consultation. C.C., S.W. wrote the manuscript. M.N. and S.-P.F. supervised the project. All authors discussed the

results and commented on the manuscript. C.C. and S.W. contributed equally to this work.

Competing interests Conflict of Interest

The authors declare no competing interests.

Supplementary information

Supporting information available.

- Figure S1 (Scanning electron microscope images), supplementary notes 1-3 (Estimated ideal efficiency, calculation of experimental efficiency, details of computational model).
- Video of discharging demonstration.

Source data

Source data available.

Data availability

All data supporting the findings of this study are available from the Source Data. Source data are provided with this paper.

References

[1] C. Haddad, C. Périlhon, A. Danlos, M.-X. François, G. Descombes, Some Efficient Solutions to Recover Low and Medium Waste Heat: Competitiveness of the Thermoacoustic Technology, Energy Procedia. 50 (2014) 1056–1069. https://doi.org/10.1016/j.egypro.2014.06.125.

[2] E. Ruiz-Casanova, C. Rubio-Maya, J.J. Pacheco-Ibarra, V.M. Ambriz-Díaz, C.E. Romero, X. Wang, Thermodynamic analysis and optimization of supercritical carbon dioxide Brayton cycles for use with low-grade geothermal heat sources, Energy Conversion and Management. 216 (2020) 112978. https://doi.org/10.1016/j.enconman.2020.112978.

[3] Y. Chen, P. Lundqvist, A. Johansson, P. Platell, A comparative study of the carbon

dioxide transcritical power cycle compared with an organic rankine cycle with R123 as working fluid in waste heat recovery, Applied Thermal Engineering. 26 (2006) 2142–2147. https://doi.org/10.1016/j.applthermaleng.2006.04.009.
[4] M. Rahimi, A.P. Straub, F. Zhang, X. Zhu, M. Elimelech, C.A. Gorski, B.E. Logan, Emerging electrochemical and membrane-based systems to convert low-grade heat to electricity, Energy Environ. Sci. 11 (2018) 276–285. https://doi.org/10.1039/C7EE03026F.
[5] C. Cheng, Y. Dai, J. Yu, C. Liu, S. Wang, S.P. Feng, M. Ni, Review of Liquid-Based Systems to Recover Low-Grade Waste Heat for Electrical Energy Generation, Energy Fuels. 35 (2021) 161–175. https://doi.org/10.1021/acs.energyfuels.0c03733.
[6] H. Ma, X. Wang, Y. Peng, H. Peng, M. Hu, L. Xiao, G. Wang, J. Lu, L. Zhuang, Powerful Thermogalvanic Cells Based on a Reversible Hydrogen Electrode and Gas-Containing Electrolytes, ACS Energy Lett. 4 (2019) 1810–1815. https://doi.org/10.1021/acsenergylett.9b00944.
[7] J. Duan, G. Feng, B. Yu, J. Li, M. Chen, P. Yang, J. Feng, K. Liu, J. Zhou, Aqueous thermogalvanic cells with a high Seebeck coefficient for low-grade heat harvest, Nat Commun. 9 (2018) 5146. https://doi.org/10.1038/s41467-018-07625-9.
[8] I. Burmistrov, N. Kovyneva, N. Gorshkov, A. Gorokhovsky, A. Durakov, D. Artyukhov, N. Kiselev, Development of new electrode materials for thermo-electrochemical cells for waste heat harvesting, Renewable Energy Focus. 29 (2019) 42–48. https://doi.org/10.1016/j.ref.2019.02.003.
[9] W. Liu, Q. Jie, H.S. Kim, Z. Ren, Current progress and future challenges in thermoelectric power generation: From materials to devices, Acta Materialia. 87 (2015) 357–376. https://doi.org/10.1016/j.actamat.2014.12.042.
[10] B. Yu, J. Duan, H. Cong, W. Xie, R. Liu, X. Zhuang, H. Wang, B. Qi, M. Xu, Z.L. Wang, J. Zhou, Thermosensitive crystallization–boosted liquid thermocells for low-grade heat harvesting, Science. 370 (2020) 342–346. https://doi.org/10.1126/science.abd6749.
[11] L. Zhang, T. Kim, N. Li, T.J. Kang, J. Chen, J.M. Pringle, M. Zhang, A.H. Kazim, S. Fang, C. Haines, D. Al- Masri, B.A. Cola, J.M. Razal, J. Di, S. Beirne, D.R. MacFarlane, A. Gonzalez- Martin, S. Mathew, Y.H. Kim, G. Wallace, R.H. Baughman, High Power Density Electrochemical Thermocells for Inexpensively Harvesting Low- Grade Thermal Energy, Adv. Mater. 29 (2017) 1605652. https://doi.org/10.1002/adma.201605652.
[12] C. Gao, Y. Yin, L. Zheng, Y. Liu, S. Sim, Y. He, C. Zhu, Z. Liu, H.-W. Lee, Q. Yuan, S.W. Lee, Engineering the Electrochemical Temperature Coefficient for Efficient Low-Grade Heat Harvesting, Adv. Funct. Mater. 28 (2018) 1803129. https://doi.org/10.1002/adfm.201803129.
[13] Y. Yang, J. Loomis, H. Ghasemi, S.W. Lee, Y.J. Wang, Y. Cui, G. Chen, Membrane-Free Battery for Harvesting Low-Grade Thermal Energy, Nano Lett. 14 (2014) 6578–6583. https://doi.org/10.1021/nl5032106.
[14] S.W. Lee, Y. Yang, H.-W. Lee, H. Ghasemi, D. Kraemer, G. Chen, Y. Cui, An electrochemical system for efficiently harvesting low-grade heat energy, Nat Commun. 5 (2014) 3942. https://doi.org/10.1038/ncomms4942.
[15] C. Cheng, S. Wang, P. Tan, Y. Dai, J. Yu, R. Cheng, S.-P. Feng, M. Ni, Insights into the Thermopower of Thermally Regenerative Electrochemical Cycle for Low Grade Heat Harvesting, ACS Energy Lett. (2020) 329–336. https://doi.org/10.1021/acsenergylett.0c02322.
[16] X. Wang, Y.-T. Huang, C. Liu, K. Mu, K.H. Li, S. Wang, Y. Yang, L. Wang, C.-H.

Su, S.-P. Feng, Direct thermal charging cell for converting low-grade heat to electricity, Nat Commun. 10 (2019) 4151. https://doi.org/10.1038/s41467-019-12144-2.
[17] K. Mu, Y. Mu, X. Wang, X. Wu, C. Pang, Y.-T. Huang, S.-P. Feng, Direct Thermal Charging Cell Using Nickel Hexacyanoferrate (II) Anode for Green Recycling of Low-Grade Heat, ACS Energy Lett. 7 (2022) 1146–1153. https://doi.org/10.1021/acsenergylett.2c00057.
[18] F. Zhang, J. Liu, W. Yang, B.E. Logan, A thermally regenerative ammonia-based battery for efficient harvesting of low-grade thermal energy as electrical power, Energy Environ. Sci. 8 (2015) 343–349. https://doi.org/10.1039/C4EE02824D.
[19] W. Wang, H. Tian, G. Shu, D. Huo, F. Zhang, X. Zhu, A bimetallic thermally regenerative ammonia-based battery for high power density and efficiently harvesting low-grade thermal energy, J. Mater. Chem. A. 7 (2019) 5991–6000. https://doi.org/10.1039/C8TA10257K.
[20] X. Zhu, M. Rahimi, C.A. Gorski, B. Logan, A Thermally-Regenerative Ammonia-Based Flow Battery for Electrical Energy Recovery from Waste Heat, ChemSusChem. 9 (2016) 873–879. https://doi.org/10.1002/cssc.201501513.
[21] C. Cheng, S. Wang, Y. Wu, I.T. Bello, Y. Dai, R. Cheng, S. Zhai, Y. Wang, S.-P. Feng, M. Ni, Thermally Regenerative CO_2 -Induced pH-Gradient Cell for Waste-to-Energy Conversion, ACS Energy Lett. 6 (2021) 3221–3227. https://doi.org/10.1021/acsenergylett.1c01000.
[22] J.-G. Shim, D.W. Lee, J.H. Lee, N.-S. Kwak, Experimental study on capture of carbon dioxide and production of sodium bicarbonate from sodium hydroxide, Environmental Engineering Research. 21 (2016) 297–303. https://doi.org/10.4491/eer.2016.042.
[23] L. Liu, Y. Liu, C. Liu, Enhancing the Understanding of Hydrogen Evolution and Oxidation Reactions on Pt(111) through Ab Initio Simulation of Electrode/Electrolyte Kinetics, J. Am. Chem. Soc. 142 (2020) 4985–4989. https://doi.org/10.1021/jacs.9b13694.
[24] K. Nakata, Y. Kayama, K. Shimazu, A. Yamakata, S. Ye, M. Osawa, Surface-Enhanced Infrared Absorption Spectroscopic Studies of Adsorbed Nitrate, Nitric Oxide, and Related Compounds 2: Nitrate Ion Adsorption at a Platinum Electrode, Langmuir. 24 (2008) 4358–4363. https://doi.org/10.1021/la703476m.
[25] R. Cheng, M. Shi, Sulfate-induced electrochemical instability in the transpassive region during the electrooxidation of Na2S on Pt, J Solid State Electrochem. 23 (2019) 1523–1531. https://doi.org/10.1007/s10008-019-04234-4.
[26] R. Dalbeck, W. Vielstich, Ex situ analysis of sulfate adsorption on platinum via thermal desorption spectroscopy in ultra high vacuum, Electrochimica Acta. 40 (1995) 2687–2688. https://doi.org/10.1016/0013-4686(95)00124-W.
[27] F. Gossenberger, F. Juarez, A. Groß, Sulfate, Bisulfate, and Hydrogen Co-adsorption on Pt(111) and Au(111) in an Electrochemical Environment, Front. Chem. 8 (2020) 634. https://doi.org/10.3389/fchem.2020.00634.